Inviscid Modeling of Turbomachinery Wake Transport

H.D. Joslyn,* J.R. Caspar,† and R.P. Dring‡
United Technologies Research Center, East Hartford, Connecticut

The problem of unsteady wake-airfoil interaction and wake transport is of importance in nearly all fluid mechanical devices involving rotating machinery. In this study, an inviscid airfoil-to-airfoil potential flow analysis is used to predict the transport of the wakes of upstream stators through both rotating compressor and turbine airfoil passages. In the analysis, the wakes are assumed to have an infinitesimal velocity defect and are represented by inviscid flow streamlines. The dependence of wake rotation on airfoil lift and the dependence of wake distortion on airfoil geometry are both shown. Flow visualization results obtained in both a large-scale compressor and a large-scale turbine show good comparison with the predictions of the inviscid model.

Nomenclature

b_x = cascade axial chord
C = absolute frame velocity
C_x = absolute frame axial velocity
s = distance along a streamline
s^* = arc length along airfoil surface
t = time
U_m = rotor wheel speed at midspan
V = relative velocity
x = axial distance
y = tangential distance
β = relative flow angle
Γ = airfoil circulation
ϕ = flow coefficient (C_x/U_m)
Φ = potential function
τ = cascade pitch

Introduction

THE physics of unsteady wake-airfoil interaction and wake transport through airfoil rows has a significant impact on turbomachinery component aerodynamic efficiency,[1] airfoil heat transfer,[2] and structural loading.[3] In particular, relative to stationary cascade results, unsteadiness due to wake-airfoil interactions in turbines can result in increases of nearly 50% in airfoil aerodynamic loss,[4] 40% in average external airfoil heat transfer,[5] and 20% in airfoil unsteady structural loading.[6] The interaction of an upstream stator wake with a downstream rotating airfoil row is related to the manner in which the wake fluid is transported through the rotating airfoil passages. Therefore, to develop an analytical model of wake-airfoil interaction, it is essential not only to characterize the flow, including the wake at the inlet to the rotor, but also to determine the trajectory and distortion of the incoming wake as it convects through the rotor airfoil passage.

Benchmark data consisting of the velocity and turbulence fields upstream of, within, and downstream of compressor and turbine rotor passages would be of great value in the formulation of analytical wake-airfoil interaction predictive schemes. The acquisition of such information, however, can be extremely time consuming and expensive. Therefore, it would be very useful if, prior to such a detailed experiment, wake trajectories could be estimated with a simple analytical technique and the predicted results used to optimize the test matrix to be used in the experiment. Wagner et al.[7] and Zierke and Okiishi[8] have used simplified convection models to explain the interactions of compressor blade wakes as they progress through downstream rows. The experimental work of Hodson[9] and Binder et al.[10] indicate that wake-airfoil interaction and wake transport in turbine rotor passages can be explained using inviscid (potential flow) concepts. The present study was conducted to assess a simple analytical scheme that can be used relatively easily to predict wake trajectories in rotating airfoil rows.

The results presented were obtained by applying a two-dimensional potential flow calculation to predict idealized wake trajectories through compressor and turbine airfoil row geometries. By "idealized" we mean wakes with a negligible velocity defect. Therefore, in the analysis, the wakes are modeled as inviscid flow streamlines in the absolute frame of reference. The calculation also predicts the time lag or separation distance (drift) between the fluid particles on the stagnation streamline as they "split" and pass over the upper (suction) and lower (pressure) surfaces of the airfoil.

Included in the present study are the analytical results for a second-stage impulse turbine rotor,[11] a large-scale single-stage compressor rotor,[12] and a large-scale, first-stage turbine rotor.[13] A flow visualization technique[14] devised to observe flowfields in rotating turbomachinery is employed to assess qualitatively the prediction for both the large-scale, single-stage compressor and first-stage turbine rotors. Absolute frame streamline trajectories are tracked in this experiment with the flow visualization technique.

The Numerical Method

Wake Transport Calculations

In the present study, the inviscid potential flow through the midspan section for each airfoil geometry is calculated using the control area method of Caspar et al.[15] The flow is assumed to be two-dimensional and incompressible. Furthermore, the wakes are assumed weak, i.e., to have zero velocity defect. Therefore, in this case, the wakes are assumed to correspond to absolute frame streamlines and the wake's position is represented by a streamline filament aligned along the wake centerline position. The cascade for the impulse turbine rotor of Ref. 11 is shown in Fig. 1. Shown are the inlet and exit relative velocities, the inlet and exit relative flow angles, and the cascade pitch. After the two-dimensional potential function is defined at the calculation grid points by the solution of the control area difference equations, the local quadratic polynomials that approximate the potential

Presented as Paper 85-1132 at the AIAA/SAE/ASME/ASEE 21st Joint Propulsion Conference, Monterey, CA, July 8-10, 1985; received July 25, 1985; revision received Nov. 5, 1985.

*Research Engineer, Gas Turbine Technology Group.
†Principal Scientist.
‡Manager, Gas Turbine Technology.

function near the grid points are defined. These are then pieced together to provide continuous approximations to the potential function and its derivatives throughout the flowfield. The relative frame stagnation streamlines are defined by integrating the equation

$$\Phi_x dy - \Phi_y dx = 0 \tag{1}$$

from the cascade airfoil leading and trailing edge stagnation points to the appropriate upstream and downstream far-field boundaries. Relative frame streamlines at specified locations between the stagnation streamlines are defined by integrating Eq. (1) from the upstream to the downstream far-field boundary. Calculated relative frame streamlines for the impulse turbine rotor passage are shown in Fig. 2, along with the initial position of an upstream wake (absolute frame streamline). The rotor inlet velocity triangle diagram is shown in the upper right-hand corner of Fig. 2.

The time it takes a fluid particle to move along a given relative frame streamline is obtained from the equation

$$t = \int ds/V \tag{2}$$

where t is the time, s the distance along the streamline, and V the relative speed,

$$V = (\Phi_x^2 + \Phi_y^2)^{1/2} \tag{3}$$

The wake trajectory curves of Fig. 3 are obtained by connecting points on the various relative frame streamlines with the same time increment value from the initial reference position of the wake ($t=0$). In this case, the initial position of the upstream wake is oriented in the absolute frame at an angle of 28.5 deg from tangential and is denoted by the thickened line labeled $t=0$ in Fig. 3. Subsequent positions (e.g., the lines labeled 1-8 in Fig. 3) show the temporal evolution of the wake trajectory as it is chopped by the rotor and is convected through the rotor passages. At position 2, the portion of the wake in the upper passage between midpitch and the pressure surface rotates counterclockwise toward the suction surface. This rotation is primarily due to variations in the passage velocity field and secondarily due to the weak influence of the rotor velocity field upstream of the rotor leading edge. At position 3, the center blade has cut the incoming wake. This produces two wake segments: one each in the upper and lower passages. At position 4, the portion of the segment in the lower passage between midpitch and the pressure surface begins to rotate counterclockwise relative to its initial orientation for the same reasons that rotation occurred in the upper passage segment at position 2. The upper passage segment is more distorted at position 4 than at 2 due to an increase in the velocity field gradient with axial distance.

After the center airfoil chops the wake, the upper and lower passage wake segments drift apart as they convect through the rotor blade row. Note that at position 5 the upper passage segment is downstream of the rotor trailing edge; however, the lower passage segment has not yet reached the trailing edge. As seen in Fig. 3, where the corresponding upper and lower wake segments at positions 6-8 terminate on the downstream stagnation streamline of the center airfoil, there is a separation or drift distance between them of approximately 20% of the airfoil axial chord. This drift distance can be related to the lift, or circulation, associated with the airfoil and will be discussed in the next section.

In a manner similar to what was done for the impulse turbine rotor (Fig. 3), trajectories of ideal wakes for the single-stage compressor rotor and the single-stage turbine rotor were also calculated. The results of these calculations will be presented later along with the results from smoke flow visualization experiments used to assess qualitatively this inviscid model of wake transport. Wake distortion, chopping,

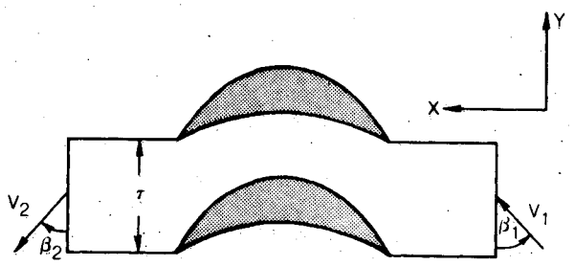

Fig. 1 Hobson impulse turbine.

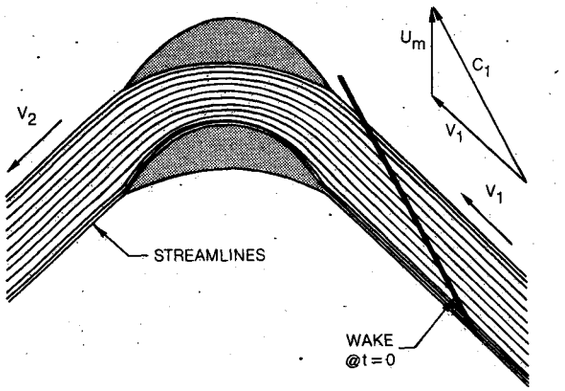

Fig. 2 Calculated relative frame streamlines for the Hobson turbine ($\phi = 1.25$).

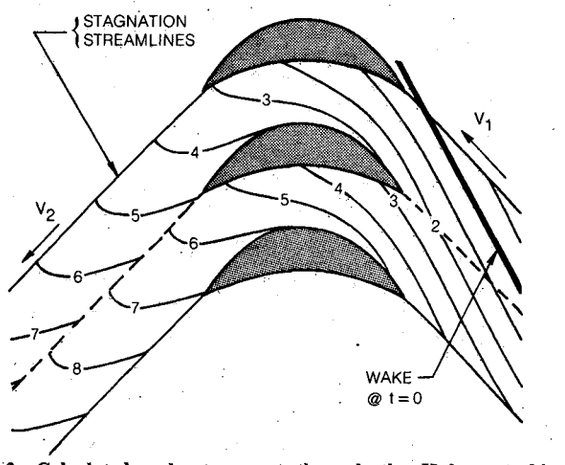

Fig. 3 Calculated wake transport through the Hobson turbine ($\phi = 1.25$).

rotation, and wake segment drift were all observed in the calculated wake trajectories for each of the three airfoil geometries examined in this study.

Drift Calculations

Two particles passing at the same time through points A and B (see Fig. 4), which are located infinitesimally close to the airfoil leading-edge stagnation streamline, will traverse the upper and lower airfoil surfaces, respectively, at different speeds. As a result, they will drift apart and will arrive at the trailing-edge stagnation point at different times. For a given airfoil geometry, the time required for the particles to travel from the leading-edge stagnation point, along the upper and lower airfoil surfaces and along the downstream stagnation streamline are, respectively,

$$t_u = \int \frac{ds}{V} \quad \text{and} \quad t_l = \int \frac{ds}{V} \tag{4}$$

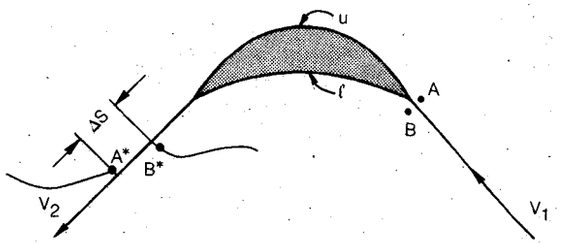

Fig. 4 Particle drift on airfoil stagnation streamlines.

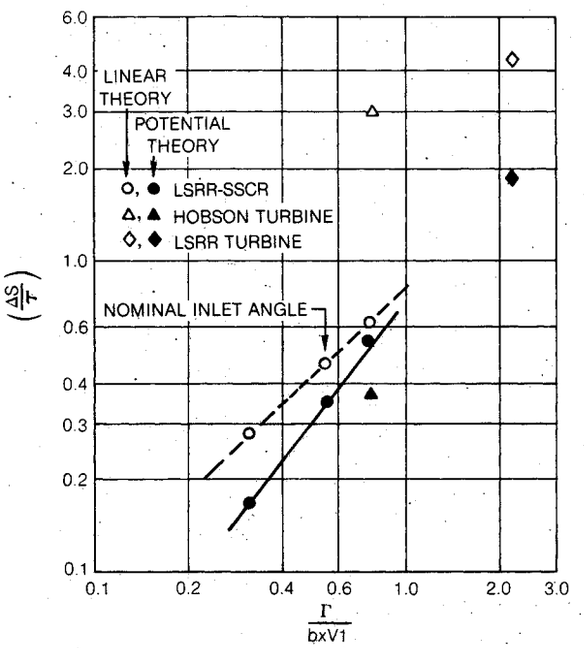

Fig. 5 Drift parameter variation with circulation.

These integrals are evaluated using the velocities obtained from the two-dimensional potential flow solution.

The drift time (that is, the time lag between the arrival at the airfoil trailing edge of one particle and then the other) causes the two particles to be separated as they travel along the downstream stagnation streamline. The separation distance varies with the flow speed and becomes constant when the flow speed becomes uniform in the streamwise direction. In the downstream region where the flow speed is uniform, the separation distance is referred to as the drift distance, denoted as Δs in Fig. 4. Locations A* and B* in Fig. 4 represent the locations of two particles on the downstream stagnation streamline. The drift distance Δs, expressed in terms of the drift time, $t_u - t_\ell$, is

$$\Delta s = (t_u - t_\ell) \cdot V_2 \tag{5}$$

Dividing the above equation by the calculation cascade pitch, the nondimensional drift distance is

$$\frac{\Delta s}{\tau} = \left(\frac{t_u - t_\ell}{\tau}\right) \cdot V_2 \tag{6}$$

Using linear (small-disturbance) theory Smith[16] shows the drift time for thin airfoils with relatively small turning to be related to the airfoil circulation and the vector mean of the cascade inlet and exit velocities. In this case, the nondimensional drift distance for thin airfoils can be approximated by

$$\left(\frac{\Delta s}{\tau}\right) \simeq \left(\frac{\Gamma}{V_m^2}\right) \cdot V_2 \tag{7}$$

In terms of the cascade pitch, the inlet and exit angles and axial velocity, circulation, and vector mean velocity can be expressed as

$$\Gamma = \tau C_x (\mathrm{ctn}\beta_1 - \mathrm{ctn}\beta_2) \tag{8a}$$

$$V_m = C_x \left[1 + \left(\frac{\mathrm{ctn}\beta_1 + \mathrm{ctn}\beta_2}{2}\right)^2\right]^{1/2} \tag{8b}$$

Substituting these expressions into Eq. (7) results in the following nondimensional drift relation for thin airfoils with small turning:

$$\left(\frac{\Delta s}{\tau}\right) = \left(\frac{1}{\sin\beta_2}\right)\left[\frac{\mathrm{ctn}\beta_1 - \mathrm{ctn}\beta_2}{1 + [(\mathrm{ctn}\beta_1 + \mathrm{ctn}\beta_2)/2]^2}\right] \tag{9}$$

Based on the linear theory approximations these results show that for thin airfoils with relatively small turning, the nondimensional drift distance [Eq. (7)] is proportional to the airfoil circulation and can be expressed in terms of the cascade inlet and exit angles as shown in Eq. (9).

The airfoil circulation can be obtained from the potential flow solution for the velocity as

$$\Gamma = \oint \bar{V} \cdot d\bar{s}^* = \oint \nabla\Phi \cdot d\bar{s}^* \tag{10}$$

The circulation [Eqs. (8a) and (10)] can be nondimensionalized by the cascade axial chord and the inlet velocity to yield

$$\frac{\Gamma}{b_x V_1} = \left(\frac{\tau}{b_x}\right) \sin\beta_1 (\mathrm{ctn}\beta_1 - \mathrm{ctn}\beta_2) \tag{11a}$$

$$\frac{\Gamma}{b_x V_1} = \frac{1}{b_x V_1} \oint \nabla\Phi \cdot d\bar{s}^* \tag{11b}$$

The drift parameter $\Delta s/\tau$ and the circulation were calculated using both the linear theory relations [Eqs. (9) and (11a)] and also from the potential flow solution [Eqs. (6) and (11b)]. Drift parameter variation with circulation for the impulse turbine rotor, the single-stage compressor rotor (SSCR) and the single-stage turbine rotor are shown in Fig. 5. For each of the three airfoil geometries, the open symbols denote results calculated from the linear theory, while the solid symbols denote results obtained from the potential flow solution.

For both the impulse turbine and the single-stage turbine rotor, the difference in drift parameter based on linear theory and that obtained from the potential flow calculation is significantly greater than the differences calculated for the single-stage compressor rotor. This is due to the relatively large thickness ($t/c > 0.2$) of the two turbine airfoils and also the high turning ($\Delta\beta > 90$ deg) that results in the vector mean velocity being significantly different from both the inlet and exit velocities. Both of these conditions violate the linear theory assumptions made to obtain Eq. (7). For the single-stage compressor rotor, the drift distances calculated from the linear theory and the potential flow solution are in closer agreement since in this case the airfoil is relatively thin ($t/c = 0.09$) and the turning (approximately 25 deg) is less than that for the two turbine airfoil geometries.

Varying the single-stage compressor rotor inlet angle by ± 10 deg about the nominal inlet angle results in the linear variation in calculated drift distance with circulation shown in Fig. 5. This linear variation is evident in the results obtained from both the linear theory and potential flow calculation. Nonlinear variations in drift distance with circulation were calculated for both the impulse and single-stage turbine geometries. For the sake of clarity, the results for the two turbine geometries are not presented. Note that the geometry

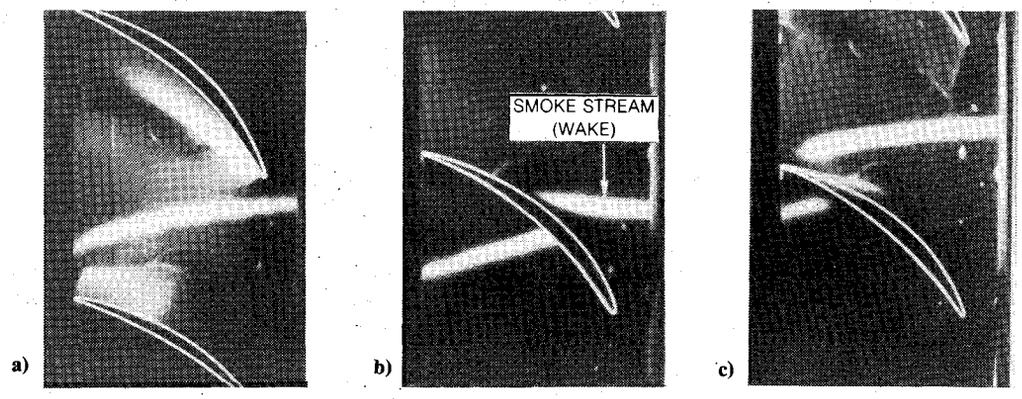

Fig. 6 Flow visualization of wake transport in a compressor rotor ($\phi = 0.85$).

with the greatest predicted drift distance is the single-stage turbine and it has the largest circulation of the three geometries examined.

Comparison with Experiment

Experimental Facility

The United Technologies Research Center large-scale rotating rig (LSRR-1) test section is 5 ft (1.52 m) in diameter and test rotors can run at speeds up to 900 rpm. Inlet flow is drawn from ambient (out-of-doors) air and the flow through the facility is essentially incompressible. Test conditions are set by the model inlet flow coefficient based on the ratio of the area average inlet axial velocity to the test rotor wheel speed at midspan. To date, 0.8 hub-to-tip radius ratio models of a 1½-stage turbine, a single-stage compressor rotor, and a two-stage compressor have been studied in detail in this facility. Detailed descriptions of the test facility, models, aerodynamic test conditions, and the dedicated on-line data acquisition and reduction system can be found in Refs. 12 and 13.

Smoke Flow Visualization Technique

Recently, a smoke flow visualization technique[14] was demonstrated that permits visualization of the flow in the rotating turbine and compressor airfoil passages. An Elvin Precision Ltd. System B smoke generator and NPL-type injector probe are used to inject smoke into the flow at midspan locations approximately four airfoil axial chords upstream of the compressor rotor and the single-stage turbine model. With this system a mineral oil, Shell "Ondina 17," is pumped to the NPL probe tip where an electrical coil heats it to produce a dense white vapor (smoke) at the injection site. For the compressor model, a single smoke injector probe was located at midspan and upstream of the rotor. To achieve high-resolution flow visualization in the turbine model, where the maximum flow speed is 200 f/s (60.9 m/s), it was necessary to inject smoke from two System B units with two NPL probes installed in tandem upstream of the stator row. This flow visualization technique produced a smoke streamer over 6 ft long that was visible to the eye and easily photographed.

A high-intensity strobe light (Strobotac model 1538A) synchronized to the test rotor through a variable time delay controller illuminated the smoke stream in a selected rotor blade passage at different circumferential positions of the rotor blade passage relative to the stationary smoke injector. The path of the smoke trace through the rotor passage was observed with a Panasonic model WV1500 black-and-white video (TV) camera and recorded on video tape with a Sony model V05850 recorder. Multiple-exposure (ensemble average) photographs were also obtained on Polaroid 600 color film in a Polaroid model 680SF camera. This was done by setting the strobe light to trigger at a selected relative rotor/injector position and then opening the camera shutter for 15 s. This procedure resulted in an ensemble average of approximately 100 exposures of the smoke stream in the same rotor passage per picture.

In the present experiment, flow visualization was employed to track absolute frame streamline trajectories, i.e., the "wakes" modeled by the inviscid analysis. A better comparison would have been obtained by tracking two-dimensional viscous wakes of the stators. However, due to the existence of a large hub-to-tip static pressure gradient at the stator exit plane of the turbine model, smoke introduced into the stator wake rapidly migrated radially toward the hub and mixed with hub end wall secondary flow vortices.

Results

Flow visualization experiments were conducted to assess qualitatively the accuracy of the potential flow wake trajectory calculations for both the single-stage compressor rotor and single-stage turbine rotor. The flow visualization results for the single-stage compressor rotor are shown in Fig. 6. The smoke streamer shown in Fig. 6 marks an absolute frame streamline which represents an ideal (zero defect) wake. The smoke was injected at midspan at a fixed location approximately four airfoil axial chords upstream of the rotor. Upstream of the compressor rotor, the absolute frame flow and hence the smoke stream (wake) trajectory is axial and proceeds from right to left. However, as seen in Fig. 6a, in going from leading to trailing edge, the wake is rotated counterclockwise in the passage. As mentioned earlier in conjunction with the calculated impulse turbine wake trajectories, this rotation is due to the relative frame velocity gradients in the passage.

In Fig. 6b, the wake is chopped by the compressor rotor and the drift of the upper wake segment relative to the lower segment on the airfoil suction and pressure surfaces respectively is evident. Recall that in the discussion of the drift calculation, it was shown (Fig. 4) that a particle on the suction surface side of the stagnation streamline would "drift" ahead of a particle on the pressure surface side if both were initially side-by-side at the airfoil leading edge. The flow visualization clearly illustrates the drift phenomenon.

In the last flow visualization picture (Fig. 6c), the chopped upper and lower wake segments are rotated and separated. The portion of the upper wake segment adjacent to the suction surface is about to exit the passage at the trailing edge, while the portion of the lower segment adjacent to the pressure surface is approximately 25% of axial chord upstream of the trailing edge.

Figure 7 shows the wake trajectories obtained from the potential flow calculation in the single-stage compressor rotor. The lines emanating from the leading and trailing

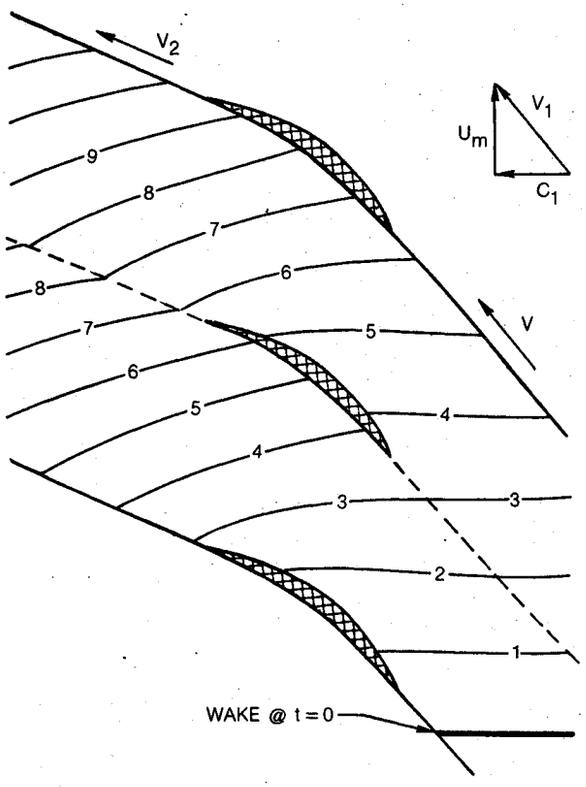

Fig. 7 Calculated wake transport through a compressor rotor ($\phi = 0.85$).

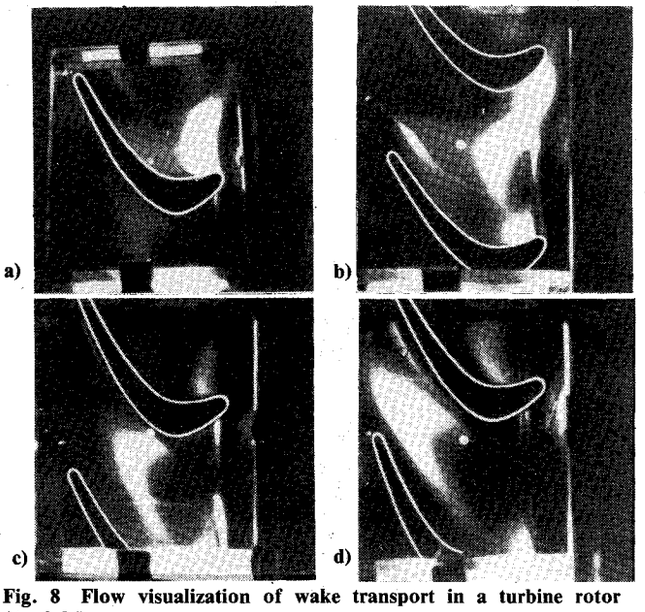

Fig. 8 Flow visualization of wake transport in a turbine rotor ($\phi = 0.34$).

edges of each airfoil are the calculated relative frame stagnation streamlines. The thick horizontal line labeled "$t = 0$" represents the initial upstream location of a wake in the absolute frame of reference. Subsequent locations (i.e., the lines labeled 1-9) of the calculated wake trajectory illustrate the phenomena of wake rotation, chopping and wake segment drift that were observed in the flow visualization experiments (Fig. 6). At position 1, there is relatively little wake rotation or distortion evident. This is due to the small change in the relative frame velocity as the leading edge of this airfoil geometry is approached from upstream by the wake. As the wake passes through positions 2 and 3, an increase in counterclockwise rotation is evident toward the suction surface due to the cross-passage velocity gradient and flow deceleration relative to the inlet velocity at these locations. The chopped wake segments at position 4 have a slight separation between them on the airfoil pressure and suction surfaces. At position 5 and beyond, the drift distance between the upper and lower passage wake segments has increased significantly to approximately one-third the cascade pitch. Qualitatively, for the single-stage compressor rotor, the inviscid calculation models the ideal wake trajectories and predicts the main features of wake rotation, chopping, and wake segment drift as observed in the flow visualization experiments.

The comparison of calculated inviscid wake transport with flow visualization results at midspan for the single-stage turbine rotor is presented in Figs. 8 and 9. Flow visualization (Fig. 8) of the inviscid upstream stator wake (smoke trace) through the rotor passage at different relative rotor/stator circumferential positions illustrates the different stages of wake distortion, chopping, and drift in the high-turning turbine passage. In the flow visualization sequence shown, the direction of rotation of the turbine airfoil row is down. The stator wake is initially oriented in the absolute frame at 15.3 deg from tangential and enters the passage shown in Fig. 8a from the upper right-hand corner. At this rotor/stator position, the wake has just entered the rotor passage and is slightly bowed. In Fig. 8b, the airfoil shown in Fig. 8a has moved down and has chopped the lower portion of the wake. The adjacent upper airfoil (Fig. 8b) has also moved down and has nearly chopped the upper portion of the wake. As the rotor airfoils continue to move down (Fig. 8c), the wake is completely chopped and the resulting wake segment is distorted (bowed). Bowing becomes more pronounced as the wake segment travels through the passage and toward the trailing edge (Fig. 8d).

It was observed that after passing through the airfoil row, the chopped wake segments emanating from the different rotor passages remained intact as they traveled downstream. If a row of stators were installed downstream of the rotor, the wake segments would enter the stator row at a fixed circumferential location relative to the leading edge of the stators. This circumferential location would depend on the relative circumferential orientation of the stators upstream and downstream of the rotor. At a particular orientation of the two stator rows, the wake segments would periodically impinge upon the leading edge of the downstream stators. This could result in significant increases in the second-stage stator aerodynamic loss and external heat transfer relative to what might be measured in a stationary cascade or at a different stator orientation.

The corresponding results from the inviscid wake trajectory calculation are shown in Fig. 9. The thick line labeled "$t = 0$" in Fig. 9 corresponds to the absolute frame location of an inviscid stator wake at a specific reference time or rotor/stator position. The other numbered lines represent the position and shape of the wake at subsequent time intervals (relative rotor/stator positions) as it is convected through the rotor passages. It is clear from the flow visualization and from the calculated results that there is considerable distortion in the form of a bowing of the wake as it proceeds from its initial position through the upper and lower passages. This is in contrast to the rotation toward the suction surface observed in the wake trajectories through both the single-stage compressor rotor and the impulse turbine (Fig. 3). Bowing of the wake in this case is due to a retardation of the incoming flow near the large leading-edge stagnation region of these airfoils, in addition to the axial and cross-passage variation in relative frame velocity.

Qualitatively, the inviscid model predicts the essential features of wake transport through the turbine rotor passage as observed in the smoke flow visualization. To assess the accuracy of the inviscid model in predicting the trajectory of

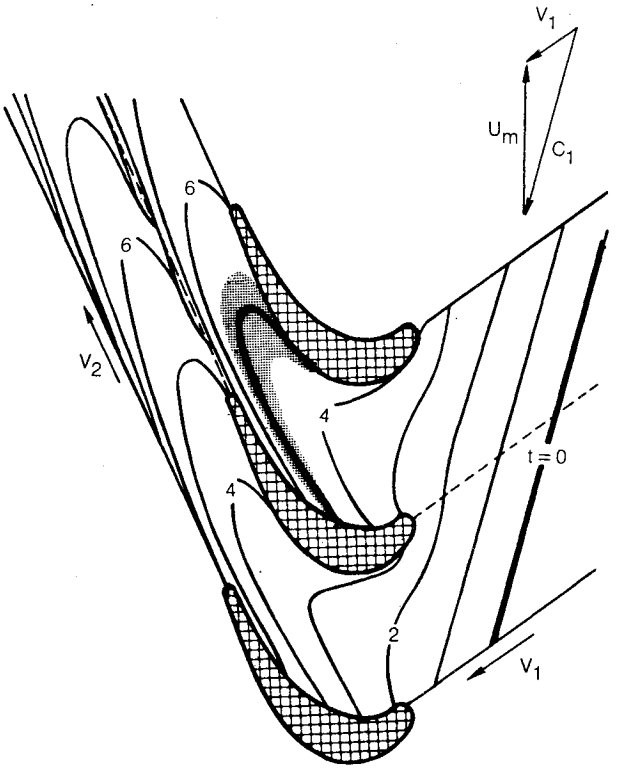

Fig. 9 Calculated wake transport in a turbine rotor ($\phi = 0.34$).

a wake modeled as an absolute frame streamline, a tracing was scaled from the flow visualization results and superimposed on the calculated results in the upper passages as shown in Fig. 9. This scaled smoke trace is indicated by the stippled area that brackets the calculated wake at position 5 in the upper passage. The calculated inviscid wake trajectory is seen to nearly evenly divide the region denoting the smoke trace.

Conclusions

An inviscid model of wake transport through rotating turbomachinery blade rows demonstrates the salient features of wake distortion (rotation and/or bowing), chopping, and wake segment drift. Calculated wake trajectories through both a single-stage compressor rotor and a single-stage turbine are in agreement with smoke flow visualization results. The principal application of this inviscid model is to estimate wake trajectories and subsequently to optimize test matrices for experimentally obtaining detailed rotor passage velocity and turbulence measurements. Although the wakes in both the analysis and experiment were represented by inviscid flow streamlines, we expect viscous wake trajectories to be similar to the inviscid streamline trajectories. However, due to the lower velocity in an actual stator wake, the bowing observed in the turbine passage is expected to be more accentuated.

Acknowledgment

This work was conducted under United Technologies Research Center corporate funding.

References

[1]Lopatitskii, A.O., et al., "Energy Losses in the Transient State of an Incident Flow on the Moving Blades of Turbine Stages," *Energomashinastroenic*, Vol. 15, No. 8, Aug. 1969.

[2]Kuhl, W. and Koschel, W., "Turbine Flow Phenomena and Their Effect on the Rotor Blade Heat Transfer," Paper presented at International Symposium on Applications of Fluid Mechanics and Heat Transfer to Energy and Environmental Problems, University of Patras, Greece, June 1981.

[3]Moses, H.L. and O'Brien, W.F., "The Chord-Wise Pressure Distribution on a Rotating Axial Flow Compressor Blade," Paper presented at 2nd International Symposium on Air Breathing Engines, Sheffield, England, March 1974.

[4]Hodson, H.P., "The Development of Unsteady Boundary Layers on the Rotor of an Axial-Flow Turbine," AGARD CP-351, June 1983, pp. 10-1—10-18.

[5]Lokay, V.I. and Trushin, T.A., "Heat Transfer from the Gas and Flow-Passage Elements of a Rotating Gas Turbine," *Heat Transfer—Soviet Research* (ASME), Vol. 2, No. 4, July 1970, pp. 108-115.

[6]Tadros, R.N. and Botman, M., "Dynamic Response of Blades and Vanes to Wakes in Axial Turbomachinery," ASME Paper 81-DET-33, 1981.

[7]Wagner, J.H., Okiishi, T.H., and Halbrook, G.J., "Periodically Unsteady Flow in an Imbedded Stage of a Multistage Axial-Flow Turbomachine," *Journal of Engineering for Power, Transactions of ASME*, Vol. 101, Jan. 1979, pp. 42-51.

[8]Zierke, W.C. and Okiishi, T.H., "Measurement and Analysis of Total Pressure Unsteadiness Data from an Axial-Flow Compressor Stage," *Journal of Engineering for Power, Transactions of ASME*, Vol. 104, April 1982, pp. 479-488.

[9]Hodson, H.P., "Measurement of Wake-Generated Unsteadiness in the Rotor Passage of Axial Flow Turbines," *Journal of Engineering for Gas Turbines and Power, Transactions of ASME*, Vol. 107, April 1985, pp. 467-476.

[10]Binder, A., Förster, W., Krause, H., and Rogge, H., "An Experimental Investigation into the Effect of Wakes on the Unsteady Turbine Rotor Flow," *Journal of Engineering for Gas Turbines and Power, Transactions of ASME*, Vol. 107, April 1985, pp. 458-466.

[11]Hobson, D.G., "Shock-Free Transonic Flow in Turbomachinery Cascades," Dept. of Engineering, University of Cambridge, England, Rept. CUED/A Turbo/TR65, 1974.

[12]Dring, R.P., Joslyn, H.D., and Hardin, L.W., "An Investigation of Compressor Rotor Aerodynamics," *Journal of Engineering for Power, Transactions of ASME*, Vol. 104, Jan. 1982, pp. 84-96.

[13]Joslyn, H.D., Dring, R.P., and Sharma, O.P., "Unsteady Three-Dimensional Turbine Aerodynamics," *Journal of Engineering for Power, Transactions of ASME*, Vol. 105, April 1983, pp. 322-331.

[14]Joslyn, H.D. and Dring, R.P., "Surface Indicator and Smoke Flow Visualization Techniques in Rotating Machinery," Paper presented at Symposium on Transport Phenomena in Rotating Machinery, Honolulu, April 1985, to be published by Hemisphere Press.

[15]Caspar, J.R., Hobbs, D.E., and Davis, R.E., "Calculation of Two-Dimensional Potential Cascade Flow Using Finite Area Methods," *AIAA Journal*, Vol. 18, Jan. 1980, pp. 103-109.

[16]Smith, L.H. Jr., "Secondary Flow in Axial-Flow Turbomachinery," *Transactions of ASME*, Vol. 77, Oct. 1955, pp. 1065-1076.